Phospholipid-independent biogenesis of a functional RP4 conjugation pilus

Naito Ishimoto[1,2,+#], Shan He[1+], Mikhail Bogdanov[3], Terry K. Smith[4], Gad Frankel[1,*], Konstantinos Beis[1,2,*]

Running title: Non-canonical conjugation pilus assembly

[1]Department of Life Sciences, Imperial College London, London SW7 2AZ, UK

[2]Rutherford Appleton Laboratory, Research Complex at Harwell, Didcot, Oxfordshire, OX11 0FA, UK

[3]Department of Biochemistry & Molecular Biology, University of Texas-Houston, McGovern Medical School, 6431 Fannin, USA

[4]BSRC, Schools of Biology and Chemistry, University of St Andrews, St Andrews, KY16 9ST, UK

[#]current address: Drug Design Laboratory, Graduate School of Medical Life Science, Yokohama City University, Tsurumi, Yokohama, 230-0045, Japan

[+]Equal contributors

Keywords: conjugative pilus; mating pair formation; cyclization; lipid-independent pilus biogenesis; phospholipids, phosphatidylglycerol

[*]Corresponding authors: g.frankel@imperial.ac.uk and kbeis@imperial.ac.uk

Abstract

Conjugation, the process of DNA transfer between bacteria, is initiated universally by the formation of a mating pair formation (MPF) via a conjugative pilus. Conjugation of the IncP RP4 plasmid is mediated by short, non-retractable, rigid mating pili. Here, we report the cryo-EM structure of the RP4 pilus at 2.75 Å resolution. Uniquely, and consistently with quantitative mass spectral analysis, this revealed that the cyclic TrbC pilin subunit is not lipidated. Consistently, an *E. coli pgsA* mutant lacking phosphatidylglycerol (PG) can serve as a donor of RP4 but not of R27, encoding the H-pilus consisting of PG-associated cyclic pilin subunits (TrhA). The RP4 is the first example of a lipid-independent functional mating pilus. This discovery not only challenges the long-held assumption that an amphipathic lipid moiety is essential for the construction of conjugative pili and for MPF, but also expanding our understanding of the diverse mechanisms that bacteria employ to transfer genetic material.

40 **Introduction**

41 Bacterial conjugation [1], [2], an efficient mechanism of horizontal gene transfer playing a central
42 role in the dissemination of antibiotic resistance, relies on extracellular appendages known as
43 conjugative pili (mating pili); these dynamic filaments mediate intercellular contacts between
44 donor and recipient bacteria and facilitate DNA transfer [3]. Studies of the archetypical F-pilus,
45 encoded by the pOX38 and pED208 plasmids, provided detailed molecular insights into the
46 pilus biogenesis process [4], [5], [6]. Briefly, the TraA pilin, which is synthesized as a pre-pilin, is
47 cleaved in the cytosol by the signal peptide peptidase LepB before it is inserted into the inner
48 membrane (IM), where it accumulates as a reservoir. While extracted from the IM the pilin co-
49 extracts phospholipids. The pilin-phospholipid complex then polymerizes into a helical
50 filament on top of the type IV secretion system (T4SS), a multi-protein complex spanning the
51 inner and outer membranes and mediating plasmid transfer [3],[4], [5], [6]. Structural studies of the
52 pOX38/pED208/pKpQIL- (IncF) [4, 7], R388- (IncW) [8], and pKM101- (IncN) [9] encoded pili
53 revealed that they are hollow helical tubes, approximately 8-10 nm in diameter, with a central
54 lumen of 2.5-3 nm, where the relaxase-bound single-stranded (ss) DNA can transverse [10]. The
55 pilins are composed of three α-helices, α1-α3, connected by short loops; the helices display
56 conformational variations in different pili. All known conjugative bacterial pili, the archaeal
57 import pili [11] and the T-pilus encoded by the Ti-plasmid of *Agrobacterium tumefaciens* [11, 9, 12]
58 have a bound phospholipid (e.g. phosphatidylglycerol – PG, phosphatidylethanolamine – PE,
59 phospholipid GDGT-0, phosphatidylcholine – PC, and C_{25}-C_{25}, C_{25}, C_{25} diether lipids) at a 1:1
60 stoichiometry with the pilin subunit. In the retractable F-pilus, the phospholipid acyl chains are
61 parallelly arranged [4], while in the unretractable R388 pilus they are splayed [8]. Cryo-electron
62 microscopy studies have shown that each TraA pilin subunit in the pilus is associated with a
63 single PG molecule [4]. The PG molecule makes extensive contact with five surrounding TraA
64 subunits, while each TraA subunit interacts with five PG molecules. Disrupting the interface

65 between the PG and the pED208 TraA pilin by site directed mutagenesis aborted pilus
66 biogenesis [4]. The phospholipids act as a "molecular glue," stabilizing the protein-protein
67 interfaces and strengthening the entire filament. This intricate network of both protein-protein
68 and protein-lipid interactions is crucial for assembling the helical filament. Stoichiometrically
69 arranged PG molecules line the TraA pilin's lumen with their solvent exposed head groups
70 directed to the interior of the pilus and the acyl chains entirely buried between protein subunits.
71 The negatively charged PG molecules-lining the pilus lumen have been suggested to neutralize
72 the positive charge of the pilus lumen, thus providing directionality for electronegative ssDNA
73 transport along the pilus interior [4] . The exception is the T pilus where the PE contributes to
74 the positive charge within the pilus lumen [11], [9].

75 We have recently reported a deviation from the prevailing model, showing that the TrhA pilin,
76 encoded by the prototype IncHI1 plasmid R27, undergoes posttranslational C-terminal
77 cleavage and cyclization [13]. Pilin cyclization is mediated via an intramolecular covalent head-
78 to-tail peptide bond between G1 and D69, forming a macrocyclic structure. The cyclic pilin is
79 lipidated and the overall pilus cryo-EM structure resembles the archetypical F-pilus [4]. Like the
80 R27 ThrA pilin, it was previously shown biochemically that the RP4 (IncP) plasmid-encoded
81 TrbC pilin is also cyclic [14], [15], [16].

82 Several studies provided detailed molecular insights into the RP4 pilus biogenesis process [14],
83 [15], [16]. Following removal of the signal peptide by LepB, maturation of TrbC requires a yet
84 unknown chromosome-encoded protease, cleaving the C-terminal 27 residues, and the
85 plasmid-encoded TraF, which while cleaving four additional C-terminal residues cyclises TrbC
86 by forming a peptide bond between S1 and G78 of the mature pilin [14], [15], [16]. Here, we report
87 the cryo-EM structure of the RP4 pilus, which unexpectedly revealed that the cyclic TrbC pilin
88 assembles into a pilus in the absence of phospholipids. Although the cyclic structure of the
89 pilin is thought to provide the pilus with greater stability, this discovery challenges the long-

90 standing model of pilus formation, where an amphipathic lipid moiety was considered essential
91 for the assembly and stability of mating pili and offers an alternative, lipid-independent pilus
92 biogenesis pathway, that diverges from the canonical model.

93

94 **Results and discussion**

95 **The cyclic TrbC pilin is assembled into a mating pilus in the absence of a phospholipid**

96 We adopted the same approach to express and purify the RP4 pilus for structural studies as we
97 reported for the H-pilus [13]. Briefly, RP4 pili were purified from *E. coli* MG1655 Δ*fimA* (lacking
98 expression of type I pili) using the needle-shaving and precipitation method (see Materials and
99 Methods) (Figure 1a). Using this method, we determined the cryo-EM structure of the RP4
100 pilus at 2.75 Å resolution (map:map FSC, 0.143 threshold) employing helical reconstruction in
101 cryoSPARC by imposing helical (rise 15.15 Å, twist 24.62°) and C5 symmetry (Figure 1b, c,
102 d and Supplementary Figure 1). The outer diameter of the pilus is ~80 Å and the lumen diameter
103 ~20 Å, comparable to other conjugation pilus structures. The Coulomb map and structure
104 confirm that the TrbC pilin is cyclized as a result of condensation of the Ser1 amine and Gly78
105 carboxyl residue and agrees with the previous biochemical studies [15] (Figure 1c). The TrbC
106 pilin contains three α-helices, α1-α3; the α1 and α2 helices are fused to form two α1/2 helices
107 connected to a split α3 helix, $\alpha3_1$ and $\alpha3_2$, through a connecting loop. This arrangement
108 resembles the conformation of the reported acyclic VirB2 pilin forming the T-pilus rather than
109 the cyclic TrhA pilin forming the H pilus that has a split α3 helix connected via a loop to α1
110 and α2 helices (Figure 2a). Although the mature cyclic TrbC pilin has an additional 10 C-
111 terminal residues compared to other pilins (Figure 2a, b), the extra residues do not impact the
112 overall structure and can be accommodated by displacement of the $\alpha3_2$ helix by 5 degrees along
113 Gly66 (Figure 2c). Unexpectedly, the structure revealed that the TrbC pilin is not associated

114 with a phospholipid. Inspection of the maps did not reveal any lipid-like electron density in the
115 proximity of the α2 or α3 helices where the bound lipids are usually located (Figure 1c, 1e, 2a).
116 We validated that no phospholipid was present by mass spectrometry analysis on lipid
117 extractions from the RP4 pilus (purified from cultures grown at either 25 or 37 C), and lipid
118 extractions from the R27 pilus, which was used as a positive control. As expected R27 derived
119 pili, showed PG species, PG 32:1 and PG 34:1, similar to those previously observed [13], while
120 the lipid extract from RP4 pili showed a complete absence of lipids under two growth
121 temperatures (Figure 3 and Supplementary Figure 2).

122 The lack of an associated phospholipid is unexpected as all pilus structures reported to date
123 have been shown to be associated with inner membrane lipids needed for biogenesis. In the
124 lipidated pilins, the phospholipid mediate contacts with neighboring pilin subunits that provide
125 extra stability in addition to the intermolecular interactions (Figure 2c). The hydrophobic
126 residues in TraA (pED208/F pilus) and ThrA (R27/H pilus) interact with the phospholipid acyl
127 chain (Figure 2c). In contrast, interactions of the TrbC protomers are mediated primarily by
128 intermolecular van der Waals forces (Figure 2c). In the absence of a bound phospholipid in the
129 protomer interface, α3 and α2' from the next protomer, of the TrbC protomers come closer to
130 'fill-in' the space in the absence of a phospholipid via a tight α3 and α2' interface; this results
131 in an offset of the two adjacent TrbC protomers by 24° rotation and 15 Å rigid body shift
132 relative to the VirB2/ThrA protomers (Figure 2c). TrbC also makes extensive interactions with
133 6 surrounding subunits whereas in lipidated-pilus structures the associated phospholipids are
134 found at the pilin interfaces (Figure 2c). The presence of different phospholipid headgroups
135 facing the lumen of pili change their overall charge from electropositive towards to
136 neutral/slight electronegative (Figure 1d, 1e). As the lumen of the lipid-free RP4 pilus is
137 inherently negatively charged this could potentially negates the need for a negatively charge
138 from the PG. The presence of a PE lipid in the T-pilus lumen results in alternating positive to

139 negative charge; this may be because the T pilus transports diverse range of substrates beyond
140 DNA [11].

141 **An *E. coli pgsA* mutant can serve as a donor of RP4 but not R27**

142 To confirm the dispensable role of glycerophospholipids in RP4 pili assembly and function,
143 we utilized a viable *pgsA* null UE54 mutant [17], [18], [19], completely lacking PG, as a donor.
144 Conjugation of R27 was used as a control. The *pgsA* gene encodes
145 phosphatidylglycerophosphate synthase, an enzyme that catalyzes the first committed step in
146 the synthesis of PG and cardiolipin (CL). PG is a ubiquitous negatively charged phospholipid
147 that present in almost all bacteria and performs specific head group-specific ligand functions
148 or reactions serving as biosynthetic precursor and probably fundamental for terrestrial life [20].
149 Therefore, as with the other Δ*pgsA* strains, PG-less UE54 is viable only if it carries two
150 additional gene mutations, including an *lpp* mutation necessary to prevent accumulation of the
151 nascent major outer membrane lipoprotein (Lpp), which requires PG for its modification.
152 Moreover, the Rcs phosphorelay system is constitutively activated in Δ*pgsA* mutants resulting
153 in the cell lyses at 37–42°C, which is prevented by a Δ*rcsF* mutation. The
154 triple *pgsA lpp rcsF* mutant is viable at any temperature because it overcomes both the
155 structural damage caused by the Lpp protein and the lethal Rcs temperature-sensitive stress
156 response activated by the absence of PG in the *pgsA* mutant. Despite the major alterations in
157 lipid composition UE54 cells divide and grow normally [21].

158 Although without PG and CL, the triple mutant can possesses some anionic phospholipids,
159 such as phosphatidic acid (PA) and N-acyl-phosphatidylethanolamine (N-acyl-PE) [21], PA is
160 accumulatedonly at trace amounts and N-acyl-PE is not synthesized at all in logarithmically
161 grown cells and PE account for near 99.8% in *pgsA* null UE54 (Fig. 4A). [^{32}P]PO_4-labeling in
162 conjunction with thin layer chromatography (TLC) demonstrates that the Δ*pgsA* mutant is

163 producing only PE as the major zwitterionic phospholipid (Figure 4a and Supplementary
164 Figure 3).

165 Following validation, we used the Δ*pgsA* mutant, and its parental wild type strain W3110, as
166 donors for RP4 and R27 and *E. coli* MG1655 as a recipient. While both RP4 and R27 were
167 conjugated as efficiently from W3110, RP4 but not R27 was conjugated efficiently from the
168 UE54 mutant (Fig. 4B). The fact that R27 plasmid cannot be conjugated efficiently when PG-
169 less UE54 was used as a donor confirms that its pilus exhibits high selectivity for PG and
170 presence of PG is vital for conjugation. Moreover, PG is irreplaceable/interchangeable with
171 other negatively charged lipid (PA and N-acyl PE) present in residual amounts in the *pgsA* null
172 strain.

173 The lipid-independent biogenesis of TrbC distinguishes this pilus from other conjugative pilus
174 types, as well as from the T-pilus, which is formed from the VirB2 pilin and assembles in a
175 fivefold helical arrangement that includes phospholipids, such as phosphatidylcholine, within
176 its structure. The cyclic pilins in both R27 and RP4 may contribute to pilus strength under the
177 harsh environmental conditions. However, the presence or absence of a phospholipid is not a
178 cyclic pilin feature as the R27 pilus incorporates phospholipids into its structure at a
179 stoichiometric ratio. The RP4 plasmid's TrbC protein is unique among cyclic pilins because it
180 assembles into a functional pilus without requiring a phospholipid anchor. As such, the RP4
181 pilus provides the first known example of a lipid-independent mating pilus, expanding our
182 understanding of the diverse mechanisms that bacteria employ to transfer genetic material.

183 The distinct differences between pilus structures in bacteria (cyclic and acyclic) and archaea
184 give fundamental insights into plasmid biology, pilus biogenesis, DNA transfer and evolution.
185 It remains unclear why certain pili, acyclic or cyclic, such as the F- or H-pilus, adopt a 5-fold
186 symmetry where others such as the pKpQIL pilus adopt a one-start helical symmetry [7]; this
187 plasticity in pilus architecture underscores the emergence of adaptable bacterial conjugation

188 systems throughout evolution. For pili that retract, such as the F-pilus, it has been suggested
189 that phospholipids may (i) assist in the assembly and disassembly of pilin subunits from the
190 filament by lowering the energetic cost, (ii) provide the pilus with mechanical flexibility
191 encountered in natural environments and (iii) repel negatively charged DNA and facilitate
192 relaxase-ssDNA transfer. It has been suggested that although the R388 pilus is lipidated, it does
193 not retract because of the non-canonical binding of the phosphatidylglycerol at helix α3 with
194 its acyl chains splayed; the phospholipid would have to undergo an energetically costly
195 rearrangement for the pilus to retract [8]. The absence of lipid-like electron density in the TrbC
196 maps highlights a fundamental difference in the assembly and structure of the conjugative
197 apparatus encoded by IncP plasmids, which are found in diverse bacterial species
198 (Supplementary Figure 4). The absence of bound phospholipids in RP4 pilus explains its
199 rigidity and why it is not retractable [22]. In conclusion, our data suggest that the phospholipid is
200 not needed for TrbC extraction from the inner membrane, pilus biogenesis and relaxase-ssDNA
201 transfer. Taken together, our finding of phospholipid-independent biogenesis redefines the role
202 of phospholipids in conjugation pilus biogenesis and DNA transfer.
203
204
205 **Acknowledgements**

206 We thank Prof Christopher Thomas, University of Birmingham, for providing us with the IncP
207 plasmid. We thank Prof Edward Egelman, University of Virginia, for critical reading of the
208 manuscript. We would like to acknowledge Diamond for access and support of the cryo-EM
209 facilities at the UK national electron Bio-Imaging Centre (eBIC) under visit BI33230. This
210 project made use the Computing Platform for Electron Microscopy at Imperial College funded
211 by the BBSRC Mid-range equipment Initiative 22ALERT (BB/X019284/1). This work was
212 also supported by National Institutes of General Medical Sciences Grant R01GM121493-6 to

213 MB. NI is funded by a Fellowship from The Naito Foundation. GF is supported by a Wellcome
214 Trust Investigator Award grants 224282/Z/21/Z.

215 **Author contributions**

216 KB and GF conceived and supervised the study. NI purified the RP4 pilus, determined the
217 cryo-EM structure and performed model building and refinement. SH conducted conjugation
218 assays. MK generated and analyzed the Δ*pgsA* mutant. TKS performed the lipidomics assays
219 NI, GF and KB analyzed the structures. NI, MK, GF and KB wrote the manuscript.

220

221 **Competing interests**

222 The authors declare no competing interests.

223

224 **Materials and Methods**

225 **Expression and purification of RP4 pilus**

226 The RP4 pilus was purified following the protocol used to prepare the H pilus [13]. Briefy,
227 bacterial cells from an overnight culture were shaved through 25 G needles 25~30 times and
228 were centrifuged at 50,000 xg for 1 h. The pilus filaments were precipitated using PEG 6,000
229 at a final concentration of 5% with stirring for 1 h, which was followed by centrifugation at
230 50,000 xg for 30 min. The supernatant was removed, and the pellet was resuspended in 200 µL
231 imaging buffer (50 mM Tris-HCL pH 8, 200 mM NaCl). The solution containing the filaments
232 was dialyzed overnight in imaging buffer. Sample purity was judged by SDS-PAGE.

233 **Grid preparation and cryo-EM data collection**

234 For grid preparation, 3 µL of the purified sample at ~4 mg/mL was applied to a glow-
235 discharged carbon grid (Quantifoil R1.2/1.3, Cu, 300 mesh). The grid was blotted with a
236 blotting force of 0 for 3 sec at 4°C and 100% humidity, and flash-frozen in liquid ethane using
237 a Vitrobot Mark IV (Thermo Fisher Scientific). Cryo-EM data were collected on 300 kV Titan
238 Krios G2 (Thermo Fisher Scientific) with a Falcon 4i detector and Selectris X energy filter at
239 the Electron Bioimaging Center (eBIC), UK. A total of 3,405 movies were collected at a
240 magnification of ×130,000 (pixel size of 0.921 Å/pixel) with a total electron dose of 50 e/Å2.
241 The defocus range was set between -0.8 and -1.8 µm. All data were automatically acquired
242 using EPU software. The data collection parameters are summarized in Supplementary Table
243 1.

244 **Cryo-EM data processing and model building**

245 The collected data were processed using cryoSPARC (v.4.6.1) [23]. Data were collected from a
246 Titan Glacios and Krios, analyzed separately, and 2D images and initial volume from Glacios
247 dataset were used for initial reconstruction. Both datasets were processed following similar

248 steps. Motion correction was performed using Patch Motion Correction, and CTF estimation
249 for micrographs was done by Patch CTF estimation [23]. Particles from the Glacios dataset were
250 manually picked from all micrographs and extracted in a binned state at 2.76 Å/pix. The
251 extracted particles were classified in two rounds in 2D classification, and selected high-quality
252 particles were used as references for the Filament tracer. Three rounds of 2D classification
253 from the whole dataset was used to select particles for helical reconstruction. Helical symmetry
254 search job suggested an axial rise of ~15.3 Å and a twist of ~24.6º, along with 5-fold point
255 group symmetry. These symmetry parameters were used as starting parameters for helical
256 reconstruction using Helix refine. 4.0 Å P-pilus map was reconstructed from Glacios data set.
257 Then, 2D references and 3D model were used for reference to Krios dataset. In Krios dataset,
258 3,405 movies were collected. After Motion Correction and CTF refinement, template pick was
259 performed with Filament tracer using a 2D reference from the Glacios dataset. 4,302,764
260 particles were extracted in the binning state. Three rounds of 2D classification were performed,
261 and 10,792 particles were selected. Using 3D volume and helical parameters from the Glacios
262 dataset, Helical refinement, local CTF refinement and Reference-based motion correction were
263 performed several times. The final RP4 pilus helical reconstruction showed 2.75 Å resolution
264 using 10,729 particles, with a rise of 15.15 Å and a twist of 24.62°.

265 *Ab initio* model building and real space refinement were performed in PHENIX [24], [25]. The
266 model was subjected to iterative cycles of refinement and manual rebuilding in COOT [26]. The
267 structural model was validated using MolProbity [27]. The processing parameters and refinement
268 statistics are summarized in Supplementary Table 1.

269 **Determination of steady-state phospholipid composition by radiolabeling**

270 To determine the steady state phospholipid composition by radiolabeling, cells were uniformly
271 labeled with 5 μCi/ml of [^{32}P]PO4 after dilution to OD_{600} of 0.05 to initiate logarithmic growth
272 after dilution of the overnight culture. Cells were harvested by centrifugation, and

273 phospholipids were extracted by acidic Bligh Dyer procedure. After labeling, cells were
274 harvested by centrifugation and resuspended in 0.2 mL of acidic solution (0.5 M NaCl in 0.1
275 N HCl). Lipids were extracted by adding 0.6 mL of solution 2 (chloroform:methanol, 1:2, v/v),
276 followed by vortexing for 30 minutes. Subsequently, 0.2 mL of resuspension buffer was added,
277 and the sample was vortexed for an additional 10 minutes. Phase separation was achieved by
278 centrifugation at 13,000 × *g* for 5 minutes. The lower chloroform phase, containing the
279 extracted phospholipids, was collected. An aliquot corresponding to approximately 1,000–
280 2,000 counts per minute (cpm) of radiolabeled phospholipid was used for thin-layer
281 chromatography (TLC) analysis. One-dimensional TLC was performed to resolve individual
282 phospholipid species. Boric acid-impregnated Merck Kieselgel 60 TLC plates (0.25 mm
283 thickness) (EMD, Gibbstown, NJ) were activated and developed with a solvent consisting of
284 chloroform:methanol:acetic acid (65:25:8 v/v). The spots were assigned to different *E. coli*
285 phospholipids based on TLC mobility (Rf values) of in-house standards and utilization of
286 different lipid mutants including viable *pssA* null and therefore not synthesizing major
287 phospholipid PE. Radiolabeled lipids were detected using a Typhoon FLA 9500
288 PhosphoImager (GE) and quantified with ImageQuant™ software. Stored images were
289 processed and quantified using ImageQuantTM software. Phospholipid content is expressed as
290 mol% of total phospholipid based on the intensity of the captured signal on the Phosphor screen
291 generated by the radiolabeled spots on the TLC plate. The results presented are representative
292 of three or more determinations. All TLC analyses were performed in at least two independent
293 experiments to ensure reproducibility.

294 **Lipid analysis of Pili by mass spectrometry**

295 Purified pili were subjected to lipid extractions as previously described [4]. Briefly purified pili
296 (~0.05 mg) were treated with phospholipase A2 (0.1 units) in PBS for 16 h at 37°C, followed

297 by heat inactivation. The remaining Bligh and Dyer extracted lipids were analyzed with a
298 Thermo Exactive Orbitrap mass spectrometer both positive and negative ion modes.

299 **Bacterial strains, growth conditions and Conjugation**

300 UE54 (*lpp*-2 Δ*ara714 rcsF*::mini-*Tn10 cam pgsA*::FRT-*kan*-FRT) is a null for the *pgsA* gene
301 and is therefore unable to synthesize phosphatidylglycerol (PG). W3110 or UE53
302 (MG1655 *lpp*-2 Δ*ara714 rcsF*::mini-*Tn10* cam) were utilized as parental strains with wild-type
303 phospholipid composition. Cells were grown in LB medium containing 10 g/L Bacto-tryptone,
304 5 g/L Bacto-yeast extract, and 10 g/L NaCl.

305 *E. coli* W3110 or UE54 containing the derepressed R27 or RP4 were used as donors (both plasmids
306 encode chloramphenicol resistance); Streptomycin (Strp) resistant *E. coli* MG1655 was used as a
307 recipient. The donor and recipients were grown in LB at 37 °C overnight, mixed in a ratio of 10:1 (R27)
308 or 1:1 (RP4), diluted 1 in 25 in PBS and 40 µL spotted onto LB agar plates (no selection). Following
309 incubation at 37 °C for 3 h, R27 conjugation was allowed to proceed overnight at 25 °C. For RP4
310 conjugation the mixture was incubated overnight at 30 °C. The conjugation mixtures were collected
311 and resuspended in 1 mL of PBS following serial dilution from 10^{-1} to 10^{-8}. For selection of
312 transconjugants, the serial dilutions were plated on LB containing 30 µg/mL chloramphenicol and 50
313 µg/mLStrp and incubating at 37 °C overnight. Data are presented as proportions of
314 transconjugants/recipients.

315

316 **Data availability**

317 The cryo-EM maps have been deposited in the Electron Microscopy Data Bank (EMDB) under
318 accession code EMD-65024. The structural coordinates have been deposited to the RCSB
319 Protein Data Bank (PDB) under the accession code 9VF4. Raw images were submitted to the
320 Electron Microscopy Public Image Archive (EMPIAR) with ID EMPIAR-XXXX.

321

322

323 **Figure Legends**

324 **Figure 1. Cryo-EM structure of the RP4 pilus**. (a) Micrograph of the straight and rigid RP4
325 pilus. (b) Cryo-EM map of RP4-pilus. One right-handed 5-start strand is shown in green and
326 the rest of the filament in grey. The pilus has an outer diameter of ~80 Å and an inner lumen
327 diameter of ~20 Å. (c) Atomic model of the RP4 pilus (left panel). The TrbC pilin is cyclic and
328 lacks a bound phospholipid as revealed by the Coulomb map. The site of cyclization is
329 indicated by an arrowhead and the residues in orange. (d) The F-pilus lumen is lined by PG
330 (indicated by red sticks) compared to the RP4 pilus. (e) The RP4 pilus lumen displays a strong
331 electronegative charge compared to the other bacterial pili that appear more neutral, whereas
332 the T pilus has an alternating positive and negative charge. The exterior of the different pili
333 displays variable charge profile.

334

335 **Figure 2. Comparison of the TrbC with other conjugative pilins.** (a) The conformation of
336 TrbC pilin resembles the VirB2. Pilins of different conjugative pili bind diverse phosholipids
337 and in different conformation. The pilin structures and their associated lipids are shown in
338 cartoon and sticks, respectively. (b) The C-terminal 27 residues of the pre-TrbC pilin are
339 cleaved by an unknown chromosomal protease (highlighted in grey) and is further processed
340 by TraF-mediated cleavage of 4 additional residues (highlighted in yellow), linked to
341 cyclisation. The C-terminus of the F- and T-pilus that is not processed. Cyclization of the R27
342 ThrA pilin involves cleavage of the last 5 residues (highlighted in yellow). (c) In the absence
343 of phospholipids, the neighbouring TrbC protomers occupy the empty lipid-space to make
344 extensive stabilizing interactions (top row) compared to the lipidated ThrA (bottom row). Each
345 pilin protomer is shown in either surface or cartoon representation and colored differently.

346

347 **Fig. 3 Mass spectrometric analysis of lipids associated with purified pili.** Negative ion
348 mode survey scans (600-1000 m/z) of lipids isolated from pili after treatment with
349 phospholipase A2 (Supplementary Figure 2 shows the 100-1000 m/z). Annotated phospholipid
350 identities were confirmed by accurate mass. (**A**) RP4 (25C) and (**B**) R27.
351
352 **Figure 4. The role of PG in RP4 conjugation**. A. Lipid analysis profiles of parental *E. coli*
353 cells with normal (1) and UE54 *pgsA* null mutant (2) with altered lipid composition. The UE54
354 (Δ*pgsA*) contains primarily PE and no detectable PG. Uniformly ^{32}P labeled phospholipids
355 were extracted and analyzed after separation by one-dimensional TLC on boric acid-
356 impregnated silica gel plates in solvent consisting of chloroform:methanol:acetic acid (65:25:8
357 v/v). B. W3110 conjugates RP4 and R27 as efficiently into an *E. coli* MG1655 recipient, while
358 UE54 conjugates RP4 but not R27. Conjugation frequency was compared by Ordinary one-
359 ANOVA followed by Dunnett's multiple comparison test. ns=not significant, ***P =
360 adjusted P < 0.0001.
361
362

363 **References**

364 1 Low, W. W. *et al.* Mating pair stabilization mediates bacterial conjugation species
365 specificity. *Nat Microbiol* **7**, 1016-1027 (2022). https://doi.org/10.1038/s41564-022-
366 01146-4

367 2 Frankel, G. *et al.* Plasmids pick a bacterial partner before committing to conjugation.
368 *Nucleic Acids Res* **51**, 8925-8933 (2023). https://doi.org/10.1093/nar/gkad678

369 3 Waksman, G. From conjugation to T4S systems in Gram-negative bacteria: a
370 mechanistic biology perspective. *EMBO Rep* **20** (2019).
371 https://doi.org/10.15252/embr.201847012

372 4 Costa, T. R. D. *et al.* Structure of the Bacterial Sex F Pilus Reveals an Assembly of a
373 Stoichiometric Protein-Phospholipid Complex. *Cell* **166**, 1436-1444 e1410 (2016).
374 https://doi.org/10.1016/j.cell.2016.08.025

375 5 Mace, K. *et al.* Cryo-EM structure of a type IV secretion system. *Nature* **607**, 191-196
376 (2022). https://doi.org/10.1038/s41586-022-04859-y

377 6 Hu, B., Khara, P. & Christie, P. J. Structural bases for F plasmid conjugation and F
378 pilus biogenesis in Escherichia coli. *Proc Natl Acad Sci U S A* **116**, 14222-14227
379 (2019). https://doi.org/10.1073/pnas.1904428116

380 7 Zheng, W. *et al.* Cryoelectron-Microscopic Structure of the pKpQIL Conjugative Pili
381 from Carbapenem-Resistant Klebsiella pneumoniae. *Structure* **28**, 1321-1328 e1322
382 (2020). https://doi.org/10.1016/j.str.2020.08.010

383 8 Vadakkepat, A. K. *et al.* Cryo-EM structure of the R388 plasmid conjugative pilus
384 reveals a helical polymer characterized by an unusual pilin/phospholipid binary
385 complex. *Structure* **32**, 1335-1347 e1335 (2024).
386 https://doi.org/10.1016/j.str.2024.06.009

387 9 Amro, J. *et al.* Cryo-EM structure of the Agrobacterium tumefaciens T-pilus reveals
388 the importance of positive charges in the lumen. *Structure* **31**, 375-384 e374 (2023).
389 https://doi.org/10.1016/j.str.2022.11.007

390 10 Williams, S. M. *et al.* Cryo-EM Structure of the relaxosome, a complex essential for
391 bacterial mating and the spread of antibiotic resistance genes. *Nat Commun* **16**, 4906
392 (2025). https://doi.org/10.1038/s41467-025-60116-6

393 11 Beltran, L. C. *et al.* Archaeal DNA-import apparatus is homologous to bacterial
394 conjugation machinery. *Nat Commun* **14**, 666 (2023). https://doi.org/10.1038/s41467-
395 023-36349-8

396 12 Kreida, S. *et al.* Cryo-EM structure of the Agrobacterium tumefaciens T4SS-associated
397 T-pilus reveals stoichiometric protein-phospholipid assembly. *Structure* **31**, 385-394
398 e384 (2023). https://doi.org/10.1016/j.str.2023.02.005

399 13 Ishimoto, N. *et al.* Cryo-EM structure of the conjugation H-pilus reveals the cyclic
400 nature of the TrhA pilin. *Proc Natl Acad Sci U S A* **122**, e2427228122 (2025).
401 https://doi.org/10.1073/pnas.2427228122

402 14 Haase, J. & Lanka, E. A specific protease encoded by the conjugative DNA transfer
403 systems of IncP and Ti plasmids is essential for pilus synthesis. *J Bacteriol* **179**, 5728-
404 5735 (1997). https://doi.org/10.1128/jb.179.18.5728-5735.1997

15 Eisenbrandt, R. *et al.* Conjugative pili of IncP plasmids, and the Ti plasmid T pilus are composed of cyclic subunits. *J Biol Chem* **274**, 22548-22555 (1999). https://doi.org/10.1074/jbc.274.32.22548

16 Eisenbrandt, R., Kalkum, M., Lurz, R. & Lanka, E. Maturation of IncP pilin precursors resembles the catalytic Dyad-like mechanism of leader peptidases. *J Bacteriol* **182**, 6751-6761 (2000). https://doi.org/10.1128/JB.182.23.6751-6761.2000

17 Kikuchi, S., Shibuya, I. & Matsumoto, K. Viability of an Escherichia coli pgsA null mutant lacking detectable phosphatidylglycerol and cardiolipin. *J Bacteriol* **182**, 371-376 (2000). https://doi.org/10.1128/JB.182.2.371-376.2000

18 Shiba, Y. *et al.* Activation of the Rcs signal transduction system is responsible for the thermosensitive growth defect of an Escherichia coli mutant lacking phosphatidylglycerol and cardiolipin. *J Bacteriol* **186**, 6526-6535 (2004). https://doi.org/10.1128/JB.186.19.6526-6535.2004

19 Bogdanov, M. *et al.* Phospholipid distribution in the cytoplasmic membrane of Gram-negative bacteria is highly asymmetric, dynamic, and cell shape-dependent. *Sci Adv* **6**, eaaz6333 (2020). https://doi.org/10.1126/sciadv.aaz6333

20 Furse, S. Is phosphatidylglycerol essential for terrestrial life? *J Chem Biol* **10**, 1-9 (2017). https://doi.org/10.1007/s12154-016-0159-3

21 Mileykovskaya, E. *et al.* Phosphatidic acid and N-acylphosphatidylethanolamine form membrane domains in Escherichia coli mutant lacking cardiolipin and phosphatidylglycerol. *J Biol Chem* **284**, 2990-3000 (2009). https://doi.org/10.1074/jbc.M805189200

22 Samuels, A. L., Lanka, E. & Davies, J. E. Conjugative junctions in RP4-mediated mating of Escherichia coli. *J Bacteriol* **182**, 2709-2715 (2000). https://doi.org/10.1128/JB.182.10.2709-2715.2000

23 Punjani, A., Rubinstein, J. L., Fleet, D. J. & Brubaker, M. A. cryoSPARC: algorithms for rapid unsupervised cryo-EM structure determination. *Nat Methods* **14**, 290-296 (2017). https://doi.org/10.1038/nmeth.4169

24 Adams, P. D. *et al.* PHENIX: a comprehensive Python-based system for macromolecular structure solution. *Acta crystallographica. Section D, Biological crystallography* **66**, 213-221 (2010). https://doi.org/10.1107/S0907444909052925

25 Afonine, P. V. *et al.* Real-space refinement in PHENIX for cryo-EM and crystallography. *Acta Crystallogr D Struct Biol* **74**, 531-544 (2018). https://doi.org/10.1107/S2059798318006551

26 Emsley, P. & Cowtan, K. Coot: model-building tools for molecular graphics. *Acta Crystallogr D Biol Crystallogr* **60**, 2126-2132 (2004).

27 Chen, V. B. *et al.* MolProbity: all-atom structure validation for macromolecular crystallography. *Acta crystallographica. Section D, Biological crystallography* **66**, 12-21 (2010). https://doi.org/10.1107/S0907444909042073

Figure 1.

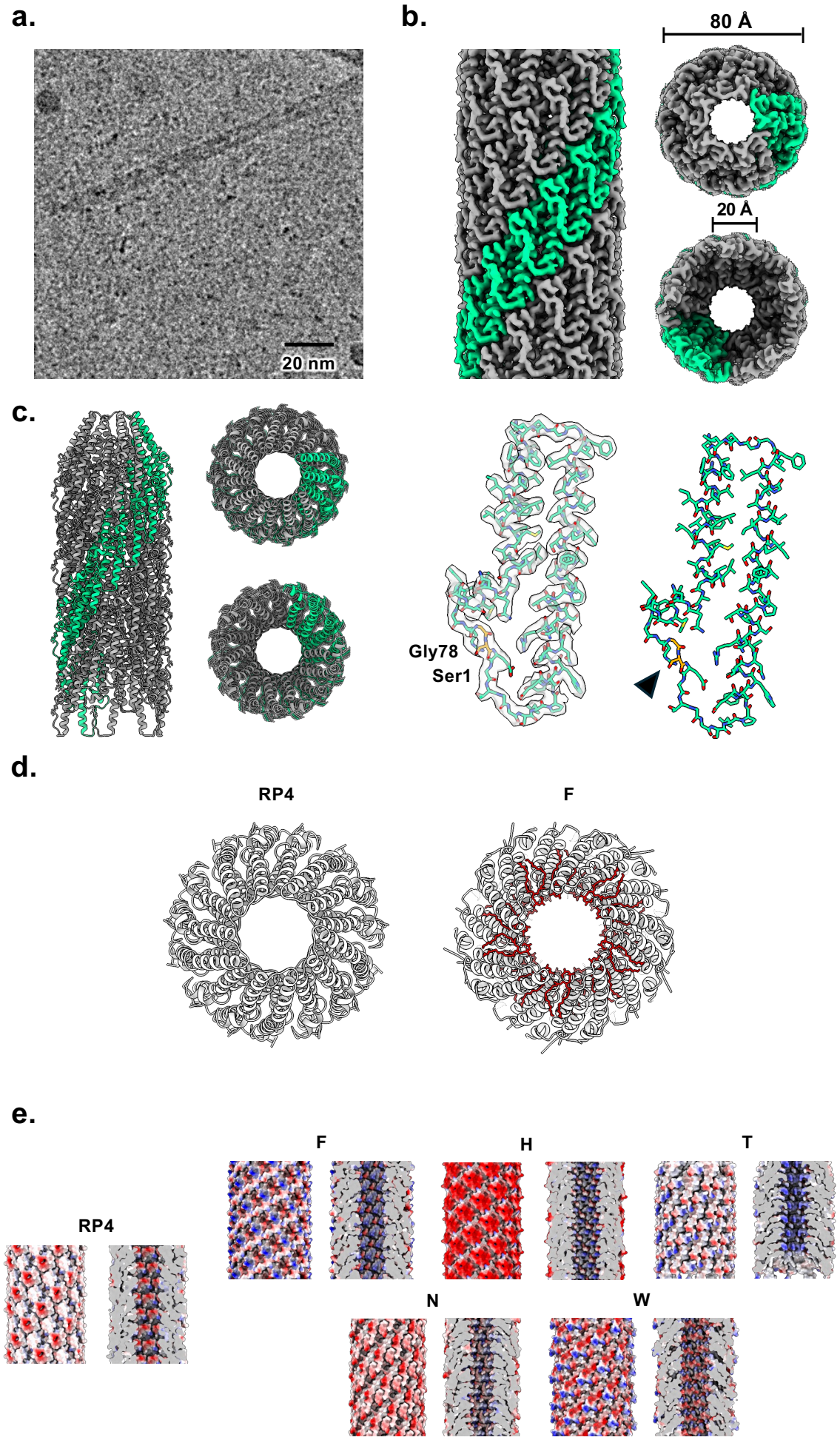

Figure 2.

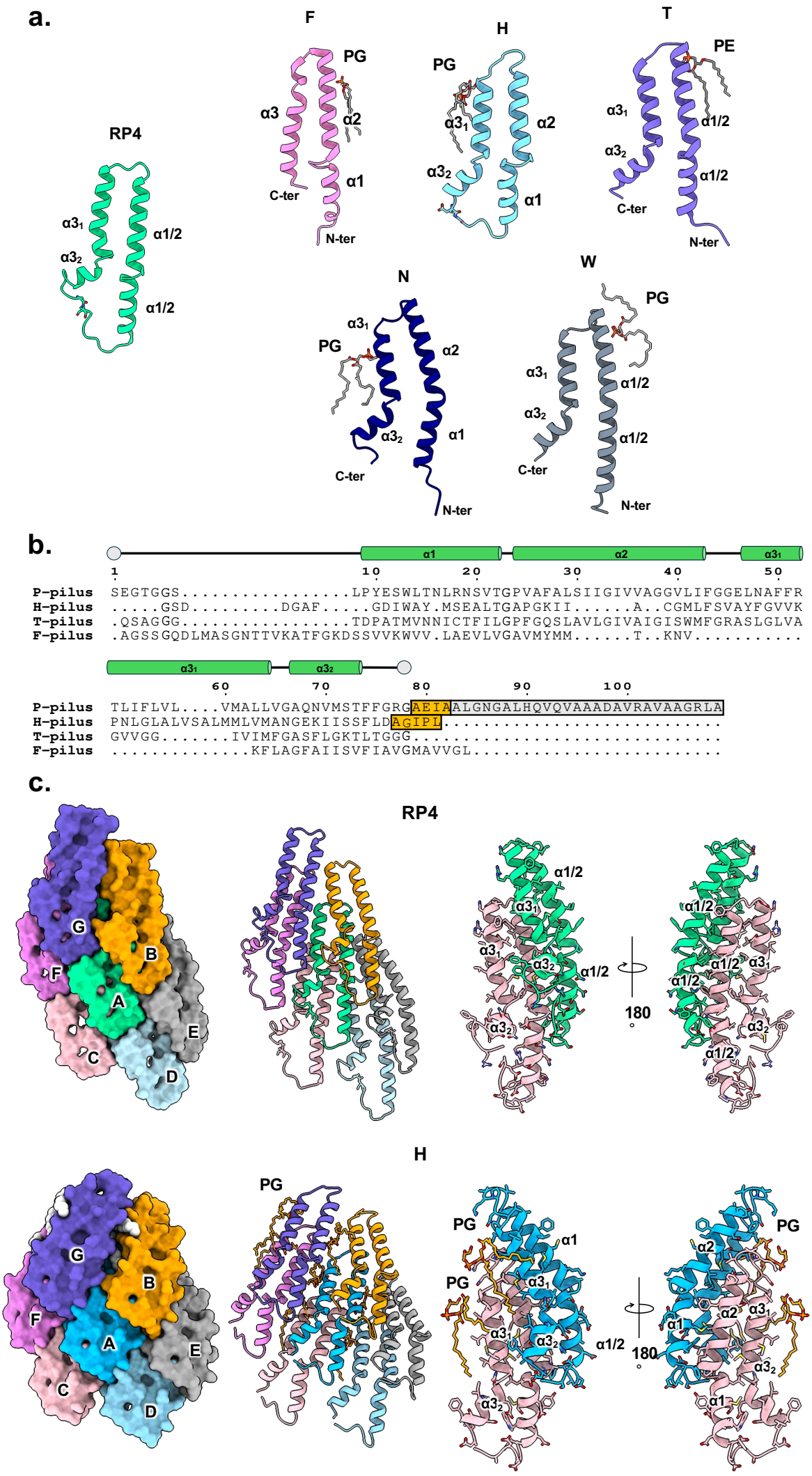
a.
RP4
α3₁
α3₂
α1/2
α1/2
F
PG
α3
α2
α1
C-ter
N-ter
H
PG
α3₁
α2
α3₂
α1
T
PE
α3₁
α1/2
α3₂
α1/2
C-ter
N-ter
N
α3₁
PG
α2
α3₂
α1
C-ter
N-ter
W
PG
α3₁
α1/2
α3₂
α1/2
C-ter
N-ter
b.
α1
α2
α3₁
1 10 20 30 40 50
P-pilus SEGTGGS.....LPYESWLTNLRNSVTGPVAFALSIIGIVVAGGVLIFGGELNAFFR
H-pilus .....GSD.....DGAF.....GDIWAY.MSEALTGAPGKII.....A..CGMLFSVAYFGVVK
T-pilus .QSAGGG.....TDPATMVNNICTFILGPFGQSLAVLGIVAIGISWMFGRASLGLVA
F-pilus .AGSSGQDLMASGNTTVKATFGKDSSVVKWVV.LAEVLVGAVMYMM.....T..KNV.....
α3₁
α3₂
60 70 80 90 100
P-pilus TLIFLVL....VMALLVGAQNVMSTFFGRGAEIAALGNGALHQVQVAAADAVRAVAAGRLA
H-pilus PNLGLALVSALMMLVMANGEKIISSFLDAGIPL.....
T-pilus GVVGG.....IVIMFGASFLGKTLTGGG.....
F-pilus .....KFLAGFAIISVFIAVGMAVVGL.....
c.
RP4
G
B
F
A
E
C
D
α1/2
α3₁
α3₁
α3₂
α1/2
α3₂
180
α1/2
α1/2
α3₁
α1/2
α3₂
α1/2
H
G
B
F
A
E
C
D
PG
PG
α1
PG
α3₁
α3₁
α3₂
α1/2
α3₂
180
PG
α2
α2
α3₁
α1
α3₂
α1

Figure 3.

a.

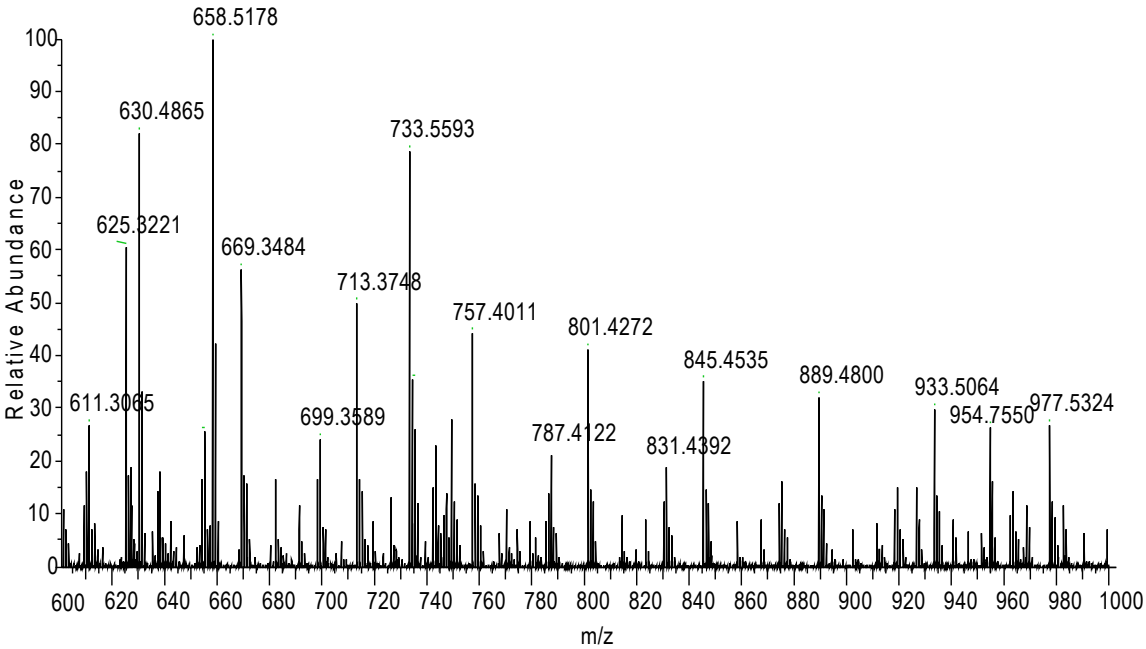
658.5178
630.4865
733.5593
625.3221
669.3484
713.3748
757.4011
801.4272
845.4535
889.4800
933.5064
954.7550
977.5324
611.3065
699.3589
787.4122
831.4392
Relative Abundance
m/z

b.

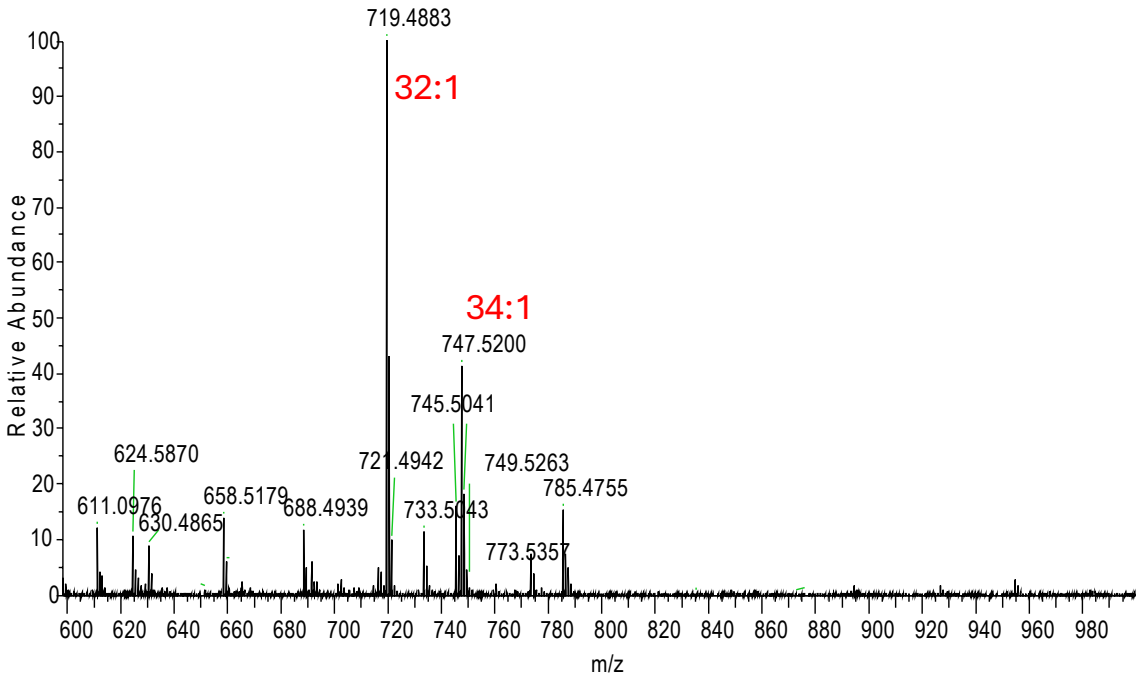
719.4883
32:1
34:1
747.5200
745.5041
624.5870
721.4942
749.5263
785.4755
611.0976
658.5179
688.4939
733.5043
630.4865
773.5357
Relative Abundance
m/z

Figure 4.

a.

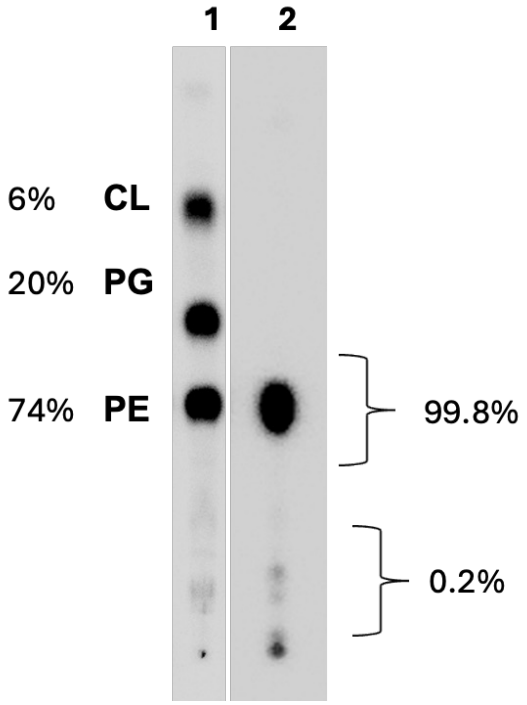
1
2
6%
CL
20%
PG
74%
PE
99.8%
0.2%

b.

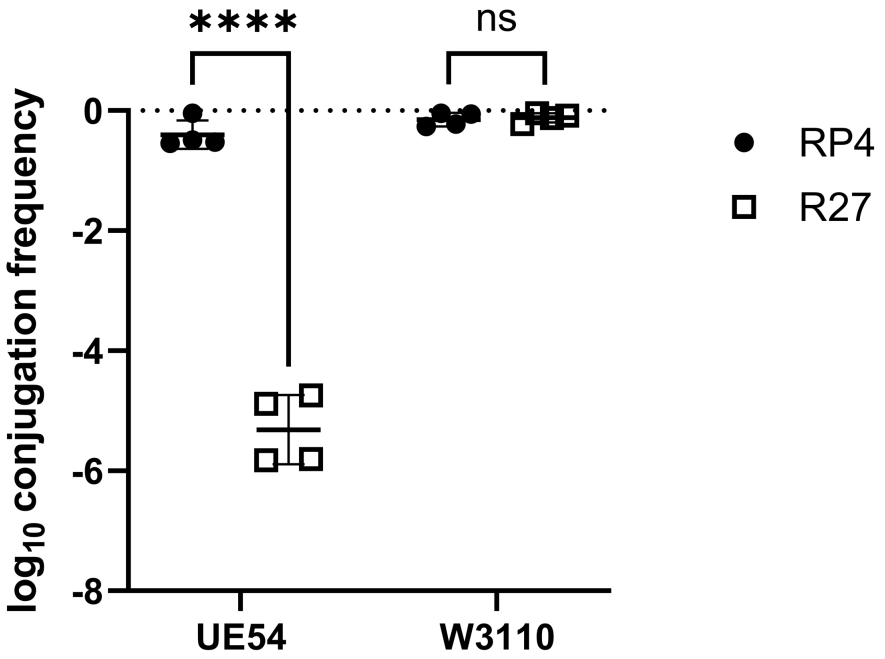
****
ns
0
-2
-4
-6
-8
log10 conjugation frequency
UE54
W3110
RP4
R27